STABILITY ANALYSIS OF THE GRAVITY ANCHORAGE OF A SUSPENSION BRIDGE BASED ON LARGE-SCALE FIELD TESTS

Zhijun Zhou[1], Chaoran Chen[1], Longfei Wang[2], Yeqing Tian[1], Hongming Feng[1] and Kangchao Wang[1]

1. *Chang'an University, School of Highway, Xi'an 710064, China; chenchaoran@chd.edu.cn,*
2. *Zhumadian Construction Survey & Design Institute Co.,Ltd., Zhumadian 463000 China; 454596968@qq.com*

ABSTRACT

The stability of gravity anchorages is critical to the safe operation of suspension bridges. The purpose of this paper is to study the stability of a gravity anchorage under the tension of main cables. Large-scale load tests and direct shear tests under the nature state and the saturated state were carried out in the adit at the bottom of the gravity anchorage, because the bottom surface of the gravity anchorage is below the design water level of a reservoir to be built. Representative rock samples in the anchorage area were selected for indoor tests. The basic parameters of the rock mass and the characteristic value of subsoil bearing capacity were obtained based on the field and indoor tests results. The static theory was used to calculate the anti-sliding stability coefficient, anti-overturning stability coefficient and contact stress of the gravity anchorage. The finite element software was used to calculate the horizontal displacement, vertical settlement and contact stress of the gravity anchorage. The calculation results met the relevant requirements, and it can be considered that the gravity anchorage was stable under the tension of main cables. It would provide a reference for the stability study of the gravity anchorage of suspension bridges.

KEYWORDS

Suspension bridge, Gravity anchorage, Anti-sliding stability, Anti-overturning stability, Contact stress

INTRODUCTION

Suspension bridges have been widely used for its beautiful shape and huge span ability. With the progress of materials and construction technology, the span of suspension bridges is increasing. At present, suspension bridges have become one of the main options for long-span bridges. As the main load-bearing structure of suspension bridges, anchorages play a role of transferring the tension of main cables to the ground. Since the main cable tension is generally large, the anchorage is the key part to ensure the stability of the suspension bridge. Due to the strong adaptability to various geological conditions and simple force transmission mechanism, the gravity anchorage is currently used in most of the built suspension bridges [1]. The stability of the gravity anchorage is related to the safe use of the suspension bridge, and it is also one of the key issues in the design of the suspension bridge [2].

Before 1960s, the gravity anchorage of long-span suspension bridges was always set on hard ground such as rock, so as to prevent the anchorage from excessive displacement or instability. In the stability calculation, it is assumed that the anchorage will not noticeably slide, sink and rotate under load [3]. Since the Verrazano Bridge was built in the United States in 1964, gravity anchorages of the suspension bridge can be built on the soil ground, allowing sinking,

strictly restricting sliding, and minimizing the overturning angle [4,5]. Taylor proposed the concept and design idea of anchorages based on its own stability in 1982 and applied it to practical engineering [6]. Andersen et al. used the limit state formula based on the working principle to evaluate the structural safety of the gravity anchorage of the suspension bridge across the eastern channel of the Great Belt [7]. Carter introduced an innovative structural concept for the design of the gravity anchorage of the Izmit Bay Bridge in high seismic area [8].

Understanding the deformation law and failure mechanism of the gravity anchorage and ground is a prerequisite for evaluating its stability [9,10]. Yin et al. study the mechanical mechanisms and failure modes of the gravity anchorage and ground by using numerical simulation [11]. They believed that the joint deformation and bearing mechanisms of the gravity anchorage and ground are comprehensively performed by friction effect, clamping effect and backfilling effect. Soil creep has a long-term effect on the stability of gravity anchorages [12]. Notched sill effect, foundation pit support and foundation reinforcement are of great significance to improve the stability of gravity anchorages [13,14]. In addition, the surrounding soil has a significant effect on improving the stability of the gravity anchorage [15]. Guo et al. use FLAC 3D modeling technology to carry out detailed numerical simulation according to the construction steps of a gravity anchorage, and analyzed the stability of the anchorage [16]. Ya et al. analysis the stability of one gravity anchorage using standard methods, shear strength reduction methods and proportionally increasing main cable tension methods and obtained the anchorage stability coefficients corresponding to different calculation methods [17].

The previous researches mainly used model tests and numerical simulations and got many interesting conclusions. However, there are few large-scale field test studies on the stability of the gravity anchorage. This paper takes the gravity anchorage of the Hutiaoxia Jinsha River Bridge as the research object. The study carried out large-scale load tests and direct shear tests in the excavated adit at the bottom of the gravity anchorage and combined with the indoor test to obtain the rock mass parameters and the characteristic value of subsoil bearing capacity. The stability of the gravity anchorage is analyzed and calculated from three aspects of anti-sliding, anti-overturning and contact stress using static theory and numerical simulation.

PROJECT DESCRIPTION

Hutiaoxia Jinsha River Bridge is a key project of Lijiang-Shangri-la expressway. The bridge spans the deep valley of Jinsha River, with a maximum height of 630.2 m. The bridge area belongs to the structurally eroded high mountain canyon landform, with a ground elevation of 1800-5600 m, a relative height difference greater than 2000 m, and a natural cross slope of 30°-60°. The total length of the bridge is 1017 m, and the main bridge is a 766 m steel truss suspension bridge. The bridge's south bank (Lijiang bank) adopts the spread foundation gravity anchorage.

The terrain on the Lijiang bank of the bridge is wide and gentle, and the vegetation on the slope is relatively developed. The slope near the anchorage is about 33°. The dynamic metamorphism of the Lijiang bank is generally strong. Schistose basalt, cleaved slate, joints of carbon phyllite are well developed, and the rock is generally broken. The stability of shallow overburden and rock slope is generally poor. The topography and landform near the gravity anchorage are shown in Figure 1(a). The distribution of the main rock layers under the gravity anchor is shown in Figure 1(b). The design elevation of the bottom of the gravity anchorage is 1998 m. The design elevation of the water level of Hutiaoxia reservoir to be built is 2010 m. Obviously, the bottom of the gravity anchorage is 12 m below the design water level.
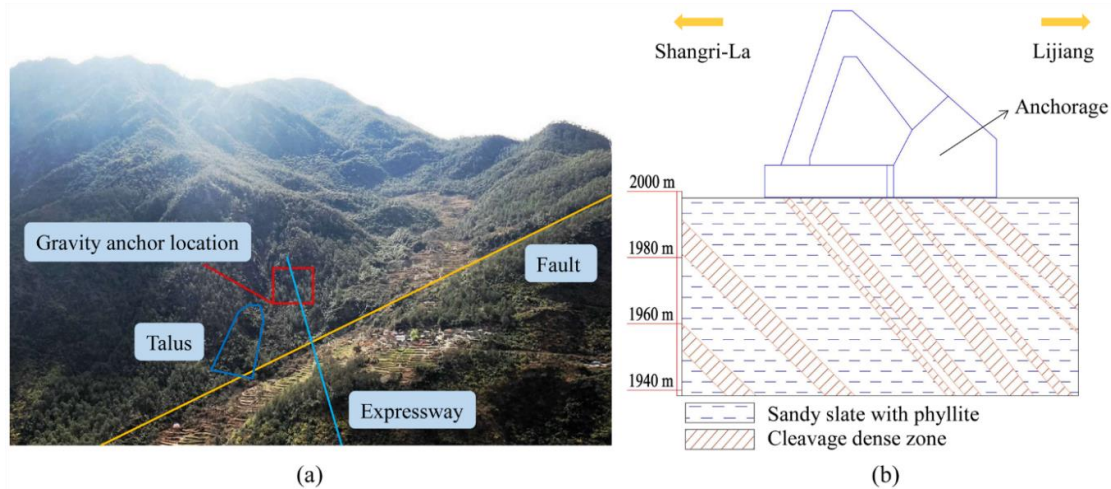
Fig. 1 - Basic information of the gravity anchorage, (a) Topography near the gravity anchor, (b) Distribution of main rock layers

The gravity anchorage adopts a frame structure. This frame type gravity anchorage effectively reduces its own gravity, reduces the stress on the ground, and reduces the amount of reinforced concrete. It has the advantages of time saving, labour saving, low cost, and beautiful appearance [18]. Therefore, most of the gravity anchorages adopt the triangular frame structure composed of a front anchor chamber, a buttress of splay saddle and anchor block.

The main structure of the gravity anchorage is shown in Figure 2(a). The gravity anchorage adopts the prestressed anchorage system, and the anchorage method adopts the front anchor type. The buttresses of splay saddle mainly bear the pressure transmitted by the saddle. The anchor block mainly bears the main cable tension transmitted by the prestressed anchorage system. The front anchor chamber is composed of side walls, roof and front walls to form a closed space, which protects the main cable strands. Because the anchor block and the side wall of the front anchor chamber mainly bear the main cable tension transmitted by the prestressed anchorage system, the concrete grade used is C40. The force of other parts of the gravity anchorage is transferred from the anchor block, and C30 concrete with lower strength grade is used.

The main dimensions of the gravity anchorage are shown in Figures 2(b) and 2(c). The total height of the gravity anchorage is 58 m, and the foundation height is 10 m. The bottom surface of gravity anchor foundation is 72 m long and 50 m wide. The design load of the main cable is 202201 kN/cable, and the horizontal incident angle of the main cable strand is 30°. The length of the main cable strand incident to the front anchor chamber is 38m, the anchorage length of the anchorage system is 20m, and the refraction angle of the main cable tension is 47°.
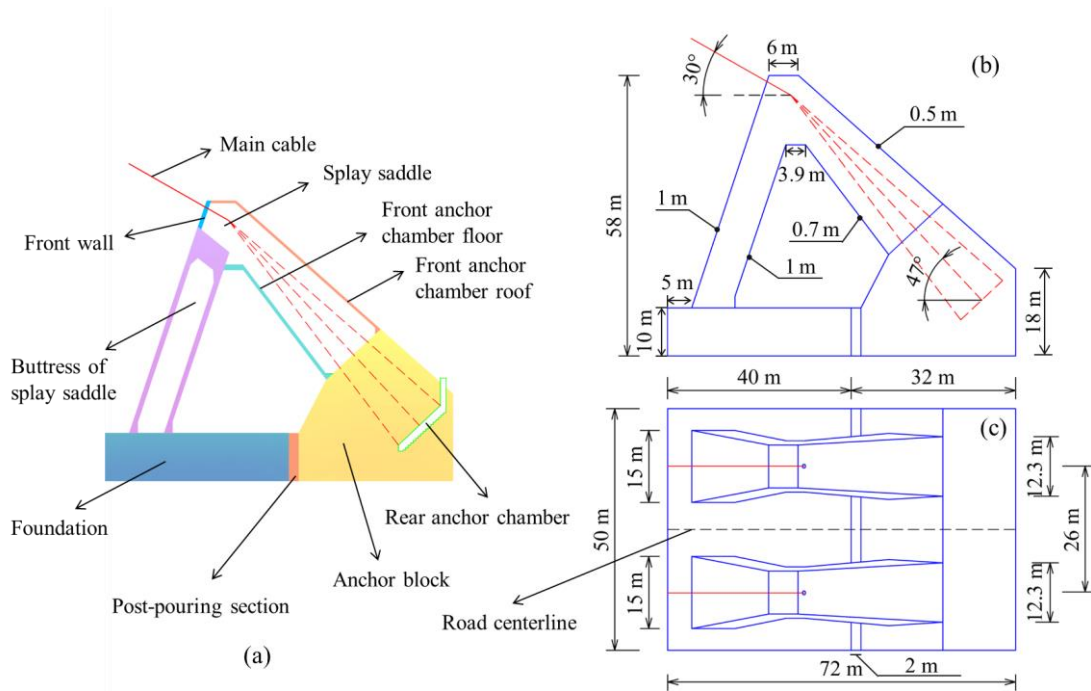
Fig. 2 - Composition and size of the gravity anchorage, (a) The main structure of the gravity anchorage, (b) Elevation of the gravity anchorage, (c) Top view of the gravity anchorage

LARGE-SCALE FIELD TEST

In order to understand the natural bearing capacity and saturated bearing capacity of the foundation under the gravity anchorage, the friction coefficient between the bottom surface of the gravity anchorage and the foundation, and the shear strength of the rock, a 50 m long adit was excavated at the bottom surface of the gravity anchorage, as shown in Figure 3(a).
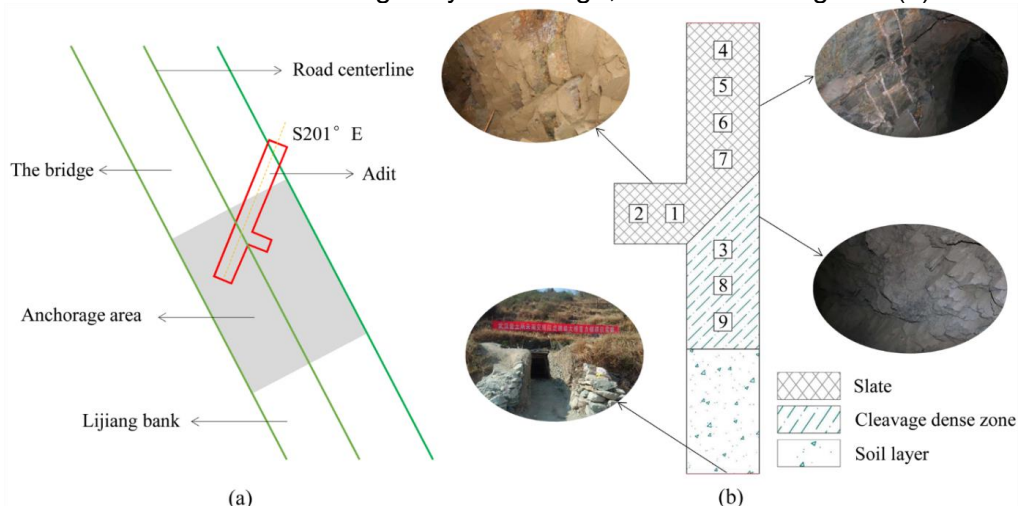
Fig. 3 - The adit location and test areas setting, (a) The adit location, (b) Test areas setting

The adit exploration reveals that the rock is a thin-thick slate, partly a cleavage dense zone, and the rock mass is relatively broken with thin phyllites. In view of the fact that the bottom of the anchorage is located 12 m below the water level of the reservoir to be built, combined with the geological conditions in the adit, a total of 9 test areas are set, as shown in Figure 3(b). Test area 1

is medium-thick layered slate. Test area 2 is thin-medium layered slate. The test areas 4, 5, 6, and 7 are thin-medium layered slate, which is intermediary weathered. The test areas 3, 8 and 9 are thin-layer slate mixed with thin-layer phyllite, which is relatively broken and is intermediary-strong weathered. Different test points were set in each test area, and the setting of test points is listed in Tables 1 and 2.

Tab. 1 - Test points of load test

Test types	Test point	Test content
Load test	1-LN	Load test in natural state
	1-LS	Load test in saturation
	2-LN	Load test in natural state
	2-LS	Load test in saturation
	3-LN	Load test in the natural state
	3-LS	Load test in saturation

Tab. 2 - Test points of direct shear test

Test types	Test point	Test content
Concrete-rock	4-SN	Shear test in natural state
	4-FN	Friction test in natural state
	4-FS	Friction test in saturation
	5-SS	Shear test in saturation
	5-FS	Friction test in saturation
	8-SS	Shear test in saturation
	8-FS	Friction test in saturation
Rock	6-SN	Shear test in natural state
	6-FN	Friction test in natural state
	7-SS	Shear test in saturation
	7-FS	Friction test in saturation
	9-SS	Shear test in saturation
	9-FS	Friction test in saturation

Load Test

Load tests were performed in representative and relatively weak positions in the adit. In order to compare the settlement deformation and consider the influence of changes of the water level, the tests were conducted in the natural state and saturated state. Load tests were carried out in accordance with the relevant specification [19]. The tests are shown in Figure 4.
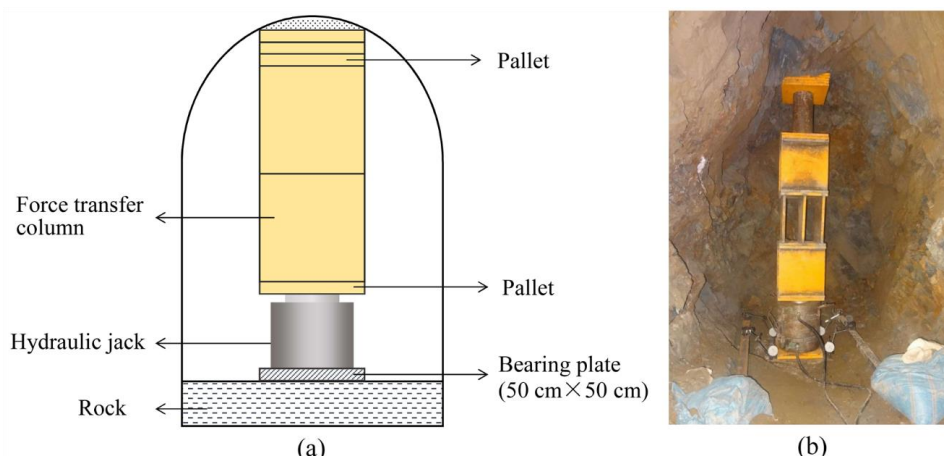
Fig. 4 - The load test, (a) Test schematic diagram, (b) Test photos

----

The deformation modulus of load test is calculated as follows:

$$E_0 = I_0 (1 - \mu^2) \frac{pd}{s} \tag{1}$$

where E_0 represents the deformation modulus of rock mass in MPa, I_0 represents the shape coefficient of the rigid bearing plate and the shape coefficient of the square bearing plate is 0.886, μ represents the Poisson's ratio of the rock mass, d is the diameter or side length of the bearing plate in m, p represents the pressure in the linear segment of the Load-Settlement curve in kPa, s is the settlement corresponding to p in mm.

The test curves are shown in Figure 5, and the test results are summarized in Table 3.
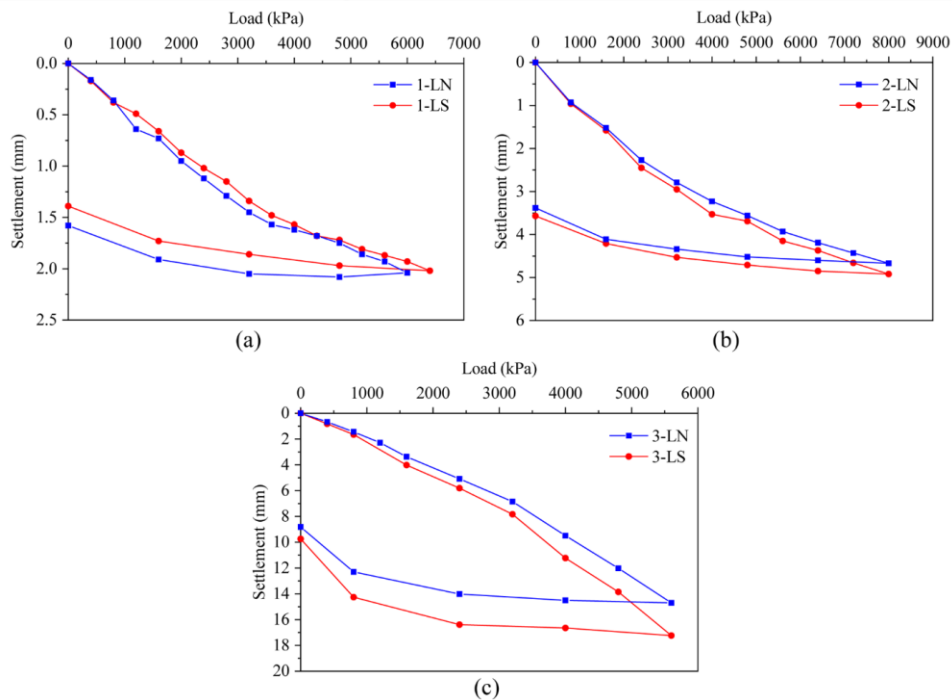
Fig. 5 - Load test curves, (a) Test curve of test area 1, (b) Test curve of test area 2, (c) Test curve of test area 3

Tab. 3 - Summary of load test results

Test point	Characteristic value of subsoil bearing capacity (kPa)	Deformation modulus		Residual deformation (mm)	Rock mass category
		0.8 MPa	3.2 MPa		
1-LN	>2213	923	916	1.58	Slate
1-LS	>2133	874	992	1.42	Slate
2-LN	>2666	358	476	3.38	Slate
2-LS	>2666	346	450	3.57	Slate
3-LN	>1866	231	194	8.82	Cleavage dense zone
3-LS	>1866	201	170	9.74	Cleavage dense zone

The load test curves (Figure 5) are basically a linear segment with no inflection points and no obvious failure conditions. The characteristic value of the bearing capacity is obtained by dividing the maximum load by 3. In the natural state and the saturated state, the bearing capacity of the rock mass in the slate area is close, as shown in Figures 5(a) and 5(b). In the cleavage dense zone, the rock mass is broken, and the settlement deformation is larger than that in the slate area, and the settlement deformation in the saturated state is larger than that in the natural state, as shown in Figure 5 (c). It can be seen from Table 3 that the characteristic value of subsoil bearing capacity in slate area is not less than 2.133 MPa, and that in cleavage dense zone is not less than 1.866 MPa. The characteristic value of bearing capacity of rock mass of the anchorage is not less than 1.866 MPa. Under the design load (0.8 Mpa), the deformation modulus of the rock mass is 201~923 MPa. Considering that the bottom surface of the anchorage is 12m below the water level of the reservoir, the deformation modulus of the slate area in saturated state is 346 MPa, and that of the cleavage dense zone is 201MPa.

Direct Shear Test

The direct shear test is divided into a shear test and a friction test. The friction test is a direct shear test in which a sample continues to be sheared along the shear plane after the sample is cut. The direct shear test is carried out according to relevant specifications [20]. The direct shear tests are shown in Figure 6.
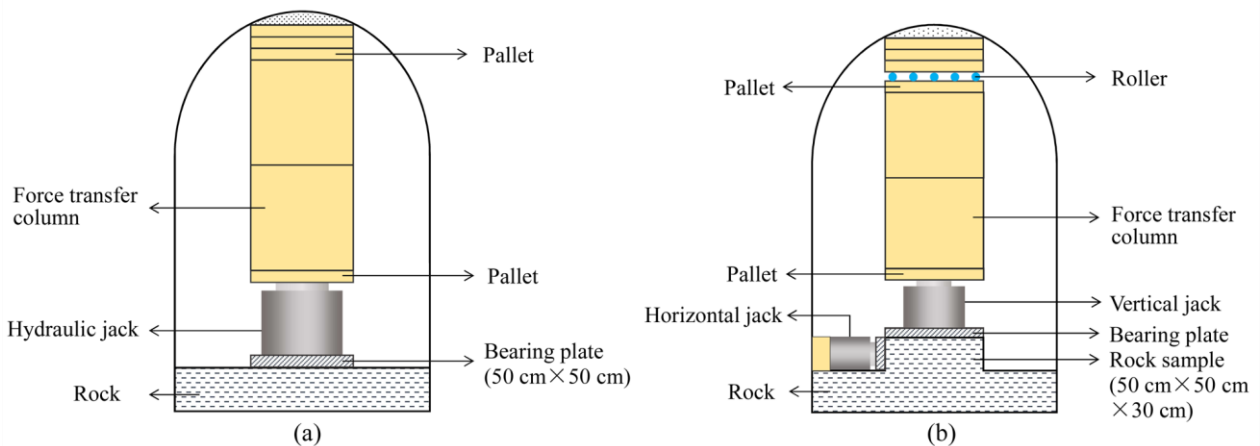
Fig. 6 - Direct shear tests, (a) The concrete-bedrock direct shear test, (b) The bedrock direct shear test

The normal pressure was applied to the sample, and the horizontal shear force was applied to the sample until it was destroyed after it was consolidated and stable. Recording the value of the shear force when the sample was destroyed and drawing the curve of shear stress τ and normal stress σ. The shear strength parameters of the rock mass can be obtained from the τ-σ curve.

The τ-σ curve follows Coulomb's law,

$$\tau = \sigma \tan \varphi + C \tag{2}$$

where τ is the shear stress acting on the shear plane in kPa, σ is the normal stress acting on the shear plane in kPa, C is the cohesion of the rock mass in kPa, φ is the internal friction angle of the rock mass in °, τ and σ can be calculated according to the following equations:

$$\sigma = \frac{P}{F} \tag{3}$$

$$\tau = \frac{Q}{F} \tag{4}$$

$$f = \tan \varphi \tag{5}$$

where P is the total normal load acting on the shear plane in kN, Q is the total shear load acting on the shear plane in kN, F is the area of the shear plane in m^2, f is the friction coefficient.

The maximum stable shear load obtained under each level of normal load was regressed to obtain the shear strength expression [21,22]. The concrete-bedrock direct shear test curves are shown in Figure 7, and the bedrock direct shear test curves are shown in Figure 8. The test results are summarized in Tables 4 and 5.
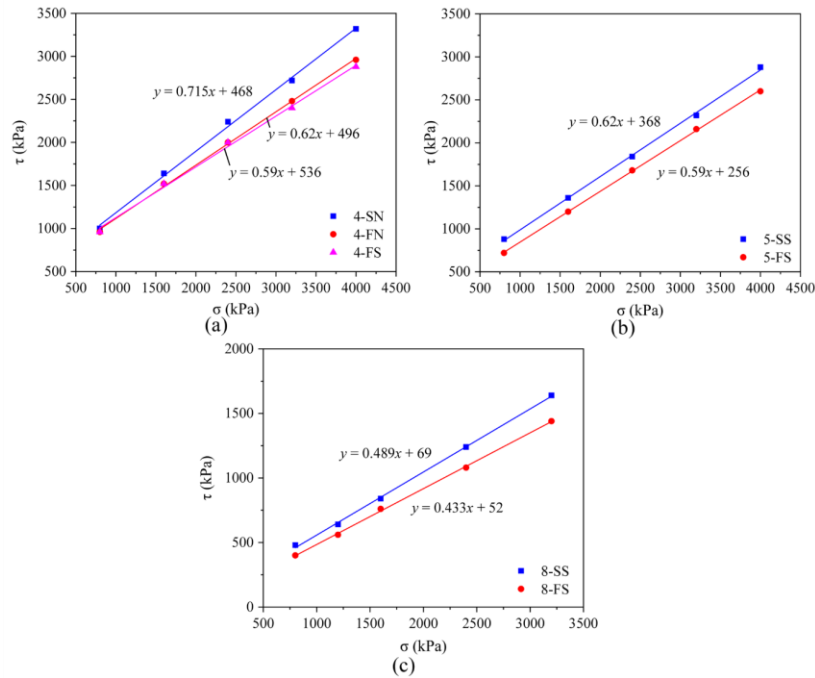
Fig. 7 - The concrete-bedrock direct shear test curves, (a) Test curve of test area 4, (b) Test curve of test area 5, (c) Test curve of test area 8
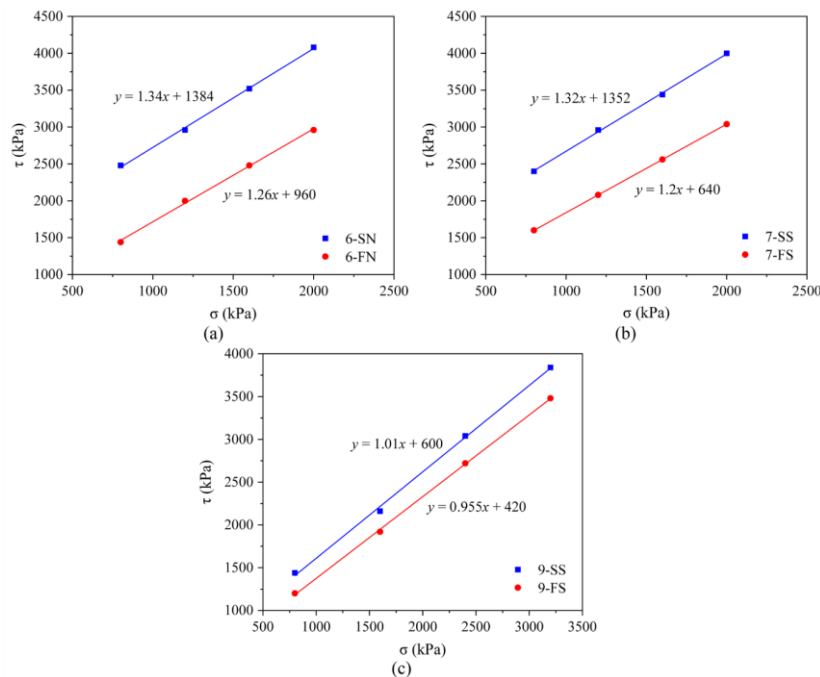
Fig. 8 - The bedrock direct shear test curves, (a) Test curve of test area 6, (b) Test curve of test area 7, (c) Test curve of test area 9

Tab. 4 - Summary of concrete-bedrock direct shear test results

Test point	Friction coefficient	Cohesion (kPa)	Rock mass category
4-SN	0.715	468	
4-FN	0.62	496	
4-FS	0.59	536	Slate
5-SS	0.62	368	
5-FS	0.59	256	
8-SS	0.489	69	Cleavage dense zone
8-FS	0.433	52	

Tab. 5 - Summary of bedrock direct shear test results

Test point	Friction coefficient	Cohesion (kPa)	Rock mass category
6-SN	1.34	1384	
6-FN	1.26	960	
7-SS	1.32	1352	Slate
7-FS	1.2	640	
9-SS	1.01	600	Cleavage dense zone
9-FS	0.955	420	

Some conclusions of the concrete-bedrock direct shear test can be obtained from Figure 7 and Table 4. The minimum friction coefficient of the test points in slate area is 0.59, which is about 26% higher than that in cleavage dense zone. The minimum cohesion of the test points in slate area is 256 kPa, which is about 5 times higher than that in cleavage dense zone. Compared with the saturated state and the natural state, the friction coefficient in the slate area decreases by about 5%, and the cohesion in the slate area increases by about 5%. The friction coefficient and cohesion of rock mass in slate area are very little affected by the water. The friction coefficient and cohesion of shear tests are larger than those of friction tests. The friction coefficients of test areas 4 and 5 are relatively small. It can be seen from the contact surface after shearing that there is residual slag on the contact surface. The friction coefficient and cohesion of the test area 8 are relatively low, because the rock mass in the cleavage dense zone is broken, and there is a lot of rock slag at the interface between the concrete and the rock mass.

Some conclusions of the bedrock direct shear test can be obtained from Figure 8 and Table 5. The minimum friction coefficient of test points in slate area is 1.2, which is about 25% higher than that in cleavage dense zone. The minimum cohesion of the test points in slate area is 640 kPa, which is about 50% higher than that in cleavage dense zone. Compared with the saturated state and the natural state, the friction coefficient of the slate area is reduced by about 4%, and the cohesion of the slate area is reduced by about 33%. The friction coefficient and cohesion in the test areas 6 and 7 are relatively high, mainly due to the steep slope of the slate layer, which intersects the shear plane at a large angle. The rock mass parameters of test area 9 are

----

significantly lower than those of test areas 6 and 7, mainly because the test area is in a dense cleavage and the rock mass is relatively broken.

Indoor Test

In order to accurately obtain the rock mass parameters of the gravity anchorage area, it is necessary to combine the results of field tests and indoor tests. In addition, the measured rock mass parameters also need to consider certain safety reserves. The sandy slate in the anchorage area was selected as the representative rock mass for indoor tests. The sandy slate samples are selected from weakly weathered rock layers, and there are weak layers in the interlayer structure surface, and the rock mass properties are relatively poor.

The physical and mechanical properties of the sandy slate can be obtained from indoor triaxial test, direct shear test and some basic density and water content tests. Based on the comprehensive analysis of indoor and outdoor test results, the density of the sandy slate is 2.4 g/cm^3, the poisson ratio is 0.2, the internal friction angle is 26°, and cohesion is 640 kPa.

STATIC ANALYSIS

Simplified Force Model of the Gravity Anchorage

The simplified force model of the gravity anchorage is shown in Figure 9. The design load of the main cable of the gravity anchorage is 202201 kN/cable. In Figure 9, G_1 represents the weight of the pier of splay saddle, G_2 represents the weight of the foundation, G_3 represents the weight of the anchor block, G_4 represents the weight of the front anchor chamber, T_h is the horizontal component of the main cable tension, T_v is the vertical component of the main cable tension, F_r is the subgrade reaction, F_w represents the buoyancy of water, F_f represents the friction resistance and cohesion of bedrock. The forces on the anchorage are summarized in Table 6.
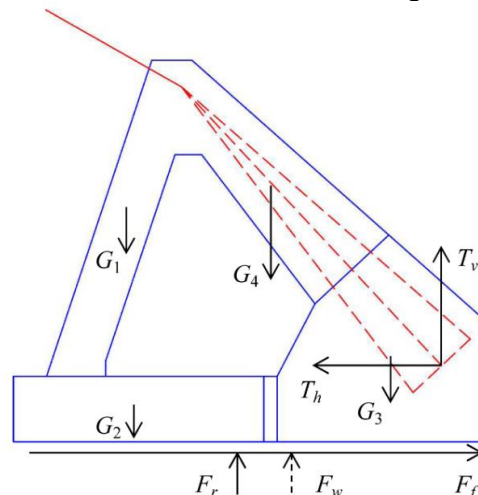
Fig. 9 - Force diagram of the gravity anchorage

Tab. 6 - Forces summary of the gravity anchorage

Force name	Force value (kN)	Arm of force to overturning axis[*] d_i (m)	Arm of force to center of gravity axis l_i (m)
G_1	0.804×10^5	23 (d_1)	11 (l_1)
G_2	5.055×10^5	20 (d_2)	16 (l_2)
G_3	8.99×10^5	56 (d_3)	21 (l_3)
G_4	1.98×10^5	38 (d_4)	4 (l_4)
F_w	0.36×10^5	36 (d_5)	0 (l_5)
T_h	2.758×10^5	12 (d_6)	12 (l_6)
T_v	2.958×10^5	62.5 (d_7)	28 (l_7)

[*] This paper takes the intersection of the bottom of the foundation and the front wall as the overturning axis.

Calculation of Anti-sliding Stability Coefficient

For the gravity anchorage with rigid enlarged foundation, the anti-sliding stability is generally calculated according to the rigid body model using the equilibrium condition. The gravity anchorage is simplified as a rigid body acting on a homogeneous ground, and only the frictional resistance between the anchorage and the ground is considered. The friction between the anchorage and the surrounding rock, as well as the rock mass resistance in the front side, are ignored as safety reserves.

The anti-sliding stability coefficient of the gravity anchor is calculated according to the following formula [19]:

$$K_a = \frac{\mu \sum P_i + \sum H_{ip}}{\sum H_{ia}} \tag{6}$$

where K_a represents the anti-sliding stability coefficient of the gravity anchorage, μ represents the friction coefficient between the bottom surface of the gravity anchorage and the ground, $\sum P_i$ is the sum of vertical forces in kN, $\sum H_{ip}$ is the sum of anti-sliding stability horizontal forces in kN, $\sum H_{ia}$ is the sum of sliding horizontal forces in kN. Substituting the relevant data into the above formula

$$K_a = \frac{\mu(G_1 + G_2 + G_3 + G_4 - F_w - T_v)}{T_h} = 2.12 > 2 \tag{7}$$

The calculated anti-sliding stability coefficient of the gravity anchorage is 2.12, which is larger than the value required by the code [23]. Therefore, the anti-sliding stability of the gravity anchorage under the tension of the main cable meets the requirement.

Calculation of Anti-overturning Stability Coefficient

The overturning mechanism of the gravity anchorage is that the anchorage will rotate with the increase of cable tension after the tension was transmitted by the cables. Moreover, the rotation direction is consistent with the cable tension direction. The rotation will eventually increase the stress in the front rock layer, and the rock layer at the posterior toe point will enter a plastic yield state, so that the ground under the anchorage will form a circular funnel-shaped sliding surface.

This paper takes the intersection of the bottom of the anchorage and the front wall as the overturning axis. The anti-overturning stability coefficient of the gravity anchorage is calculated by the following formula

----

$$K_0 = \frac{M_a}{M_c} = \frac{G_1 d_1 + G_2 d_2 + G_3 d_3 + G_4 d_4}{F_w d_5 + T_h d_6 + T_v d_7} = 3.02 > 2 \tag{8}$$

where K_0 is the anti-overturning stability coefficient of the gravity anchorage, M_a is the anti-overturning moment of force in kN·m, M_c is the overturning moment of force.

The calculated anti-overturning stability coefficient of the gravity anchor is 3.02, which is greater than the value required by the specification [23]. Therefore, the anti-overturning stability of the gravity anchorage meets the requirement.

Calculation of Subgrade Bearing Capacity

The calculation of subgrade bearing capacity requires that the contact stress does not exceed the characteristic value of subsoil bearing capacity of the bearing stratum. In the calculation, the effects of friction resistance and elastic resistance of the rock mass around the anchorage can be ignored [19].

The bearing capacity of the rock mass at the bottom of the anchorage is calculated as follows:

$$p_{max} = \frac{N}{A} + \frac{M}{W} \leq \gamma_R f_a \tag{9}$$

where p_{max} represents the maximum compressive stress on the bottom surface of the anchorage in kPa, N represents the vertical force of the bottom surface of the foundation under the action combination in kN, A is the area of the bottom of the foundation and its value is 3600 m², M is the bending moment of the external force on the anchorage to the centre of gravity axis of the anchorage in kN·m, W represents the area resistance moment in the eccentric direction of the bottom surface of the anchorage and its value is 43200 m³, γ_R represents the resistance coefficient of bearing capacity of foundation soils and its value is 1.25, and f_a represents the characteristic value of subsoil bearing capacity which is 1866 kPa from the load tests.

When the effect of water buoyancy is not considered,

$$N = G_1 + G_2 + G_3 + G_4 - T_v = 1.387 \times 10^6 \, kN \tag{10}$$

$$W = G_1 l_1 + G_2 l_2 + T_h l_6 + T_v l_7 - G_3 l_3 - G_4 l_4 = 8.934 \times 10^5 \tag{11}$$

Substituting the relevant values into Equation (9),

$$p_{max} = \frac{1.387 \times 10^6}{3600} + \frac{8.934 \times 10^5}{43200} = 405.96 \, kPa \leq \gamma_R f_a \tag{12}$$

When the effect of water buoyancy is considered,

$$N = G_1 + G_2 + G_3 + G_4 - T_v - F_w = 1.351 \times 10^6 \, kN \tag{13}$$

$$W = G_1 l_1 + G_2 l_2 + T_h l_6 + T_v l_7 - G_3 l_3 - G_4 l_4 = 8.934 \times 10^5 \tag{14}$$

Substituting the relevant values into Equation (9),

$$p_{max} = \frac{1.351 \times 10^6}{3600} + \frac{8.934 \times 10^5}{43200} = 395.96 \, kPa \leq \gamma_R f_a \tag{15}$$

The calculated maximum contact stress on the bottom of the anchorage is 405.96 kPa, which is less than the characteristic value of subsoil bearing capacity. Therefore, the subgrade bearing capacity under the pulling force of the main cable meets the requirement.

NUMERICAL SIMULATION

The contact stress, anti-sliding stability coefficient and anti-overturning stability coefficient of the gravity anchorage can be obtained through static analysis, but the horizontal displacement and vertical settlement of the gravity anchorage under the pulling force of the main cable cannot be

----

obtained. Therefore, this paper also uses finite element software Abaqus to establish a three-dimensional model of the gravity anchorage, which is used to analyze the displacement of the gravity anchorage and the contact stress under the action of main cable tension. The purpose is to further verify the stability of the gravity anchorage using finite element method based on the static analysis.

Model Establishment

Three-dimensional finite element models of the gravity anchorage and the rock mass are established. The gravity anchorage adopts the isotropic linear elastic model, and the rock mass adopts the Mohr-Coulomb model. The foundation model is set to be 288 m long, 140 m wide and 80 m high, and an excavation with a length of 72 m, a width of 50 m and a depth of 10 m is cut in the middle of it. The mesh generation of the gravity anchorage and ground is shown in Figure 10.

(a)   (b)
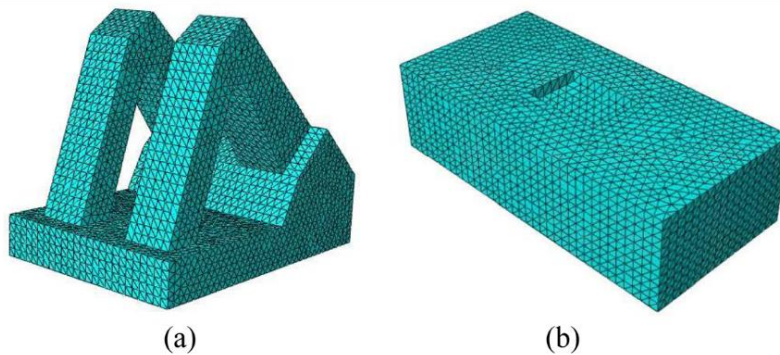
Fig. 10 - Model mesh generation, (a) Mesh generation of the gravity anchor, (b) Mesh generation of the ground

Calculation Results

Displacement Results

The gravity anchorage will be displaced horizontally under the action of the horizontal component of the main cable tension. Moreover, the oblique main cable tension will cause different settlements at the front and rear ends of the gravity anchorage, and further cause the anchorage to overturn. The horizontal sliding and the overall overturning are very detrimental to the stability of the gravity anchorage, so they must be limited in a certain range. The horizontal and vertical displacement of the gravity anchorage are shown in Figure 11.

(a)   (b)
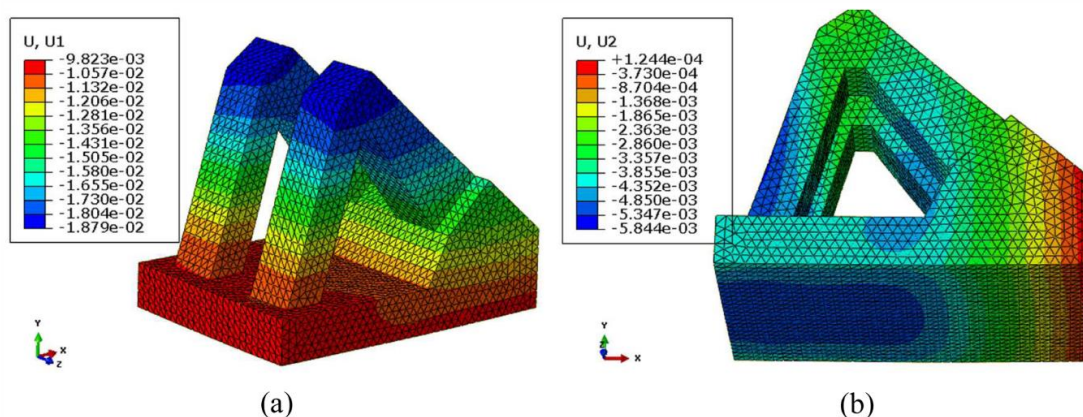
Fig. 11 - The horizontal and vertical displacements of the gravity anchorage (unit: m), (a) Horizontal displacement of the gravity anchorage, (b) Vertical displacement of the gravity anchorage

----

It can be seen from Figure 11(a) that the maximum horizontal displacement of the gravity anchorage is 18.79 mm, which occurs at the top of the side wall of the front anchor chamber. Moreover, the horizontal displacement gradually decreases from top to bottom. According to the Specification for Design of Highway Suspension Bridges [23], the allowable horizontal displacement of the gravity anchorage during the operation stage should not be greater than 0.0001 times of the main span. The calculated maximum value of 18.79 mm is smaller than the allowable value of 76.6 mm, so it meets the requirements.

As can be seen from Figure 11(b), the maximum settlement of the front end of the gravity anchorage is 5.84 mm, and the rear end is pulled up by 0.12 mm. The inclined tension of the main cable will cause the gravity anchorage to incline forward to a certain extent, resulting in uneven settlement at the front and rear ends. Therefore, the front end of the gravity anchorage may settle and the rear end may be pulled up. The specification requires that the vertical displacement of the gravity anchorage should not be greater than 0.0002 times of the main span. The calculated maximum value of 5.84 mm is less than 153.2 mm required by the specification. The overturning angle of the gravity anchor is 0.0047°, it is very small and almost negligible.

Stress Results

Because the weight of the gravity anchor is very large, it will cause very large stress on the ground. The contact stress obtained by finite element analysis is shown in Figure 12. It can be seen that the maximum compressive stress at the bottom of the anchorage is 497.6 kPa. This value is smaller than the characteristic value of subsoil bearing capacity (1866 kPa). Therefore, the contact stress under the action of the gravity anchorage meets the requirement.
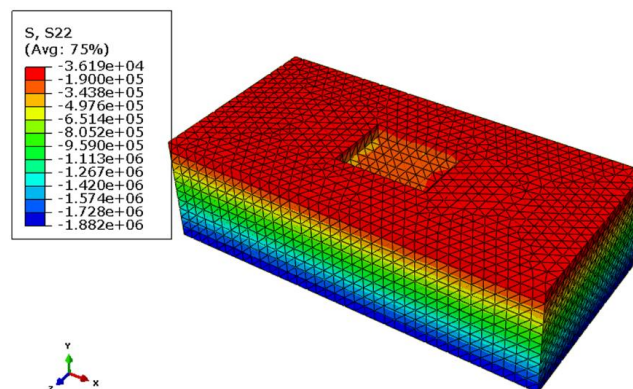
Fig. 12 - Ground stress (unit: Pa)

CONCLUSION

(1)   The basic physical parameters of the bedrock in the anchorage area can be obtained through field tests and indoor tests, including density, elastic modulus, cohesion, internal friction angle, and poisson ratio. In addition, the cohesion and friction coefficient of the contact surface between the bottom of the gravity anchorage and the bedrock, as well as the characteristic value of subsoil bearing capacity in the anchorage area are obtained. It can be concluded that the characteristic value of the subsoil bearing capacity is 1866 kPa. The deformation modulus of saturated rock mass is less than that of natural state, with a reduction of 10% ~ 20%.

(2)   The static method is used to analyze the stability of the gravity anchorage. Calculation results show that the anti-sliding stability coefficient is 2.12, the anti-overturning stability coefficient is 3.02, and the foundation stress is 405.96 kPa. The calculation results meet the relevant requirements. The anti-sliding, anti-overturning and subsoil bearing capacity of a gravity anchorage are three important aspects for checking its stability.

(3)   The stability of the gravity anchorage is analyzed by numerical simulation. The results show that the maximum horizontal displacement is 18.79 mm, the maximum vertical settlement is 5.84 mm, the maximum contact stress is 497.6 kPa, and the maximum overturning angle is 0.0047°. The calculation results meet the relevant requirements.

(4)   The gravity anchorage has a very large dead weight. In the calculation and analysis, the interaction between the bottom surface of the gravity anchorage and the ground is considered, and the shear failure of the deep rock mass is not considered. It is recommended that the shear failure of the gravity anchorage on the deep ground can be considered on the basis of meeting the stability requirements.

ACKNOWLEDGMENTS

REFERENCES

[1]   Zhang Q, Li Y, Yu M, Hu, H, Hu J, 2014. Study of the rock foundation stability of the Aizhai suspension bridge over a deep canyon area in China. Engineering Geology, 198(2015): 65–77. DOI: 10.1016/j.enggeo. 2015. 09. 012

[2]   Deng Y, Wang C, Shi Y, Liu R, 2012. Summary for Application of Super Gravity Anchorage. Highway Engineering, 37(06): 93-96.

[3]   Ge Y, Shao S, Pan H, Hu F, 2013. Deformation and safety analysis of Taizhou suspension bridge south - anchor foundation under surcharge. Science & Technology Review, 31(26): 35-39. DOI: 10.3981/j.issn.1000-7857.2013.26.004

[4]   Koji K, Fumio T, 2010. Several Geotechnical Design and Construction Issues with Akashi Strait Bridge. Soils and Foundations, 50(06): 829-845. DOI: 10.3208/sandf.50.829.

[5]   Koji M, Carlos A, Nuntikorn K, Wataru T, Kohei N, Eiji I, 2018. Performance Assessment Using Structural Analysis and Spatial Measurement of a Damaged Suspension Bridge: Case Study of Twantay Bridge, Myanmar. Journal of Bridge Engineering, 23(10): 1-14. DOI: 10.1061/(ASCE)BE.1943-5592.0001293

[6]   Taylor R J, 1982. Interaction of anchors with soil and anchor design. Naval Civil Engineering Lab, California, USA.

[7]   Andersen EY, Andreasen BS, Ostenfeld-Rosenthal P, 1992. Foundation reliability of anchor block for suspension bridge. In: Rackwitz R., Thoft-Christensen P. (eds) Reliability and Optimization of Structural Systems '91. Lecture Notes in Engineering, vol 76. Springer, Berlin, Heidelberg.

[8]   Carter M, 2012, Seismic Isolation of a Suspension Bridge Anchor Block. IABSE Congress Report, 18(12), 1235-1242.

[9]   Wu G, Zhang Y, Chen g, He S, 2013. Stress Analysis of Gravity Anchorage of Aizhai Bridge. Bridge Construction, 43(06): 40-44.

[10]   Xu S, Chen C, Zhu S, Xu F, li jie, Zhang Z, Xu T, Zhu L, 2020 Modeling Analysis of the Upper Limit Water Level Mechanism in the Upstream Reservoir of a Dam Embankment. Advances in Civil Engineering, 2020: 1-13. doi.org/10.1155/2020/8850681

[11]   Yin X, Yan F, Zhou L, Wang D, Deng Q, 2017. Joint bearing mechanism of structure and foundation for gravity anchor block of suspension bridge. Journal of Traffic and Transportation Engineering, 17(02): 1-11.

[12]   Chen T, Xiao S, Cheng Q, Zhou H, 2019. Long-term deformation and stability analysis of gravity anchorage slope on Kangding bank of Dadu River Bridge in Luding. Journal of Engineering Geology, 27(03): 632-639. DOI: 10.13544/ j.cnki.jeg.2018-253

[13]   Lai Y, Wu C, Zhang Z, 2010. Test and numerical analysis of effect of notched sill of gravity anchorage on soft rock ground of suspension bridge. Chinese Journal of Rock Mechanics and Engineering, 29(03): 593-602.

[14]   Xu T, Zhou Z, Yan R, Zhang Z, Zhu L, Chen C, Xu F, Liu T, 2020, Real-Time Monitoring Method for Layered Compaction Quality of Loess Subgrade Based on Hydraulic Compactor Reinforcement. Sensors, 20(15). DOI: 10.3390/s20154288

[15]   Luo X, 2011. Design of south anchorage foundation of Yingwuzhou Changjiang River Bridge in Wuhan. Bridge Construction, 2011(04): 05-09.

[16]   Guo S, Qi S, Li z, Ma J, Chai J, Zhai W, 2011. Stability Analysis of Anchorage for super suspension bridge over Longjiang River in Yunnan province. Journal of Engineering Geology, 19(6): 909-916.

[17]   Ya G, Han D, Shi H, Yang J, 2017. Study on the stability of gravity anchorage foundation of Nizhou Waterway Bridge of Second Humen Bridge. HIGHWAY, 62(04): 129-135.

[18]   Ma B, Ma X, Lu J, 2017. Design of anchorage and anchor system of Xiushan Bridge. Bridge Construction, 47(02): 89-94

[19]   CCCC HIGHWAY CONSULTANTS CO., LTD., 2019. Specifications for Design of Foundation of Highway Bridges and Culverts. China Communications Press Co., Ltd. Beijing, China, 73-75.

[20]   CHENDU ENGINEERING CORPORATION LIMITED, China Renewable Energy Engineering Institute, CHINA ELECTRICITY COUNCIL, 2013. Standard for test methods of engineering rock mass. China Planning Press. Beijing, China, 41-50.

[21]   Liu Y, Zhao M, Zheng S, 2011. Test study on the friction resistance of the north concrete anchor of Qingcaobei Yangtze River Bridge. JOURNAL OF CHONGQING JIAOTONG UNIVERSITY (NATURAL SCIENCE), 30(05): 911-915. DOI: 10. 3969/j. issn. 1674-0696. 2011. 05. 006

[22]   Ruan B, Xiao W, Yin H, 2011. Testing study on base resistance of the anchors at a suspension bridge. Journal of Railway Science and Engineering, 08(01): 59-62. DOI:10.19713/j.cnki.43-1423/u.2011.01.011

[23]   CCCC HIGHWAY CONSULTANTS CO., LTD., 2015. Specifications for Design of Highway Suspension Bridge. China Communications Press Co., Ltd. Beijing, China, 46-49.